

# Adsorption and Reactions of Carbon Monoxide and Oxygen on Bare and Au-Decorated Carburized W(110)

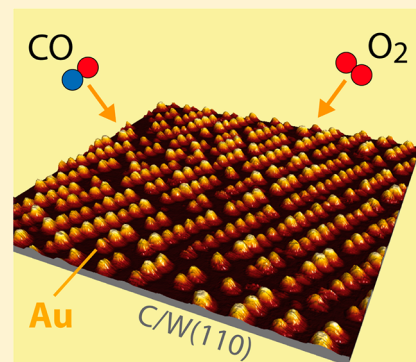
Magdalena Bachmann,<sup>†,§</sup> Djuro Bikaljevic,<sup>†,‡</sup> Norbert Memmel,<sup>\*,†</sup> and Erminald Bertel<sup>†</sup>

<sup>†</sup>Institute of Physical Chemistry, University of Innsbruck, Innrain 52a, A-6020 Innsbruck, Austria

<sup>‡</sup>Physics Department E20, Technical University of Munich, James-Franck-Str.1, D-85748 Garching, Germany

## Supporting Information

**ABSTRACT:** Adsorption and coadsorption of carbon monoxide and oxygen on different types of Au clusters on R(15 × 3)C/W(110) and R(15 × 12)C/W(110), respectively, are studied with respect to the catalytic behavior for oxidation of CO as well as of surface carbon. Carburization of the W(110) surface results in a weakening of the adsorption bond for molecularly adsorbed CO. Dissociation of carbon monoxide, which occurs on W(110), is reduced on the low-carbon coverage R(15 × 12) surface and completely suppressed on the carbon-saturated R(15 × 3) phase. Deposition of gold results in a blocking of adsorption sites for molecularly adsorbed CO and reopening of the dissociation channel. Probably the latter is associated with the existence of double-layer gold clusters and islands. At room temperature the gold clusters on both carburized templates are stable in CO atmosphere as shown by *in situ* STM measurements. In contrast, exposure to oxygen alters the clusters on the R(15 × 12) surface, implying dissociation of oxygen not only on the substrate but also on or in immediate vicinity of the gold clusters. On the Au-free carburized templates oxygen adsorbs dissociatively and is released as CO at temperatures beyond 800 K due to reaction with carbon atoms from the templates. Deposition of gold enhances the desorption rate of the formed CO at the low-temperature end of the recombinative CO desorption range, indicating a promoting effect of gold for oxidation of surface carbon. In contrast, low-temperature CO oxidation catalyzed by the deposited Au clusters is not observed. Two reasons could be identified: (1) weakly bound CO with desorption temperatures between 100 and 200 K (as reported for other related systems) is not observed, and (2) oxygen atoms are bonded too strongly to the templates.



## 1. INTRODUCTION

Haruta et al. discovered some 20 years ago that gold—known for its inert nature in the bulk state—exhibits a high reactivity as catalyst for oxidation reactions even below ambient temperatures if reduced to the size of a few nanometers.<sup>1</sup> Since then, research on Au cluster catalysis has become a subject of tremendous interest, and many reviews on this topic are available, e.g., refs 2–8. The catalytic activity of a variety of nanoparticle/support systems, such as gold on different oxides (e.g., Au/TiO<sub>2</sub>,<sup>5–13</sup> Au/MgO,<sup>3,14</sup> Au/FeO<sup>15–17</sup>) and even on inert supports,<sup>18,19</sup> has been investigated experimentally as well as by theoretical methods (e.g., refs 11, 12, 20, and 21).

However, despite 20 years of intensive research, the role of the (mostly oxidic) support as opposed to factors that are associated with intrinsic properties of the clusters remains under debate up to now.<sup>4–6,13</sup> Generally, the following issues are regarded as highly relevant for the catalytic activity and selectivity of Au: (i) Quantum size effects. In the case of gold clusters on TiO<sub>2</sub> studied by Valden et al. the maximum in the turnover frequency was observed for particles with a lateral extension of 3–3.5 nm and a thickness of 1 nm, coinciding with a metal-to-insulator transition occurring at this particle size.<sup>9</sup> Hutchings and co-workers attributed the high catalytic activity to the presence of even smaller particles (ca. 0.5 nm diameter

or 10 atoms).<sup>17</sup> The vertical extension (thickness) of the particles was supposed to be of crucial importance, as particles of bilayer height were reported to be particularly active.<sup>10,13,17</sup>

(ii) Number of low-coordinated atoms. This factor is intimately connected to the size of the particles: Generally, the number of under-coordinated Au atoms increases with decreasing size, at least if the cluster shape remains the same. This is expected to be highly relevant for the adsorption and dissociation of oxygen.<sup>4,5,15</sup> (iii) Charge of the clusters (due to interaction with the support). However, it is under debate if zerovalent gold<sup>6,22</sup> or a negative<sup>10,14,23</sup> or a positive charge<sup>24–26</sup> of the particle is required to obtain an active catalyst system. (iv) Interface effects, i.e., adsorption and activation/dissociation of oxygen at the interface between cluster and oxide.<sup>3,11,27,28</sup> Contrariwise, the studies of Chen and Goodman on a catalytically active gold bilayer on (8 × 2)-TiO<sub>x</sub>/Mo(112)<sup>10,13</sup> suggest that the interface is not directly involved in the reaction. According to their measurements, the deposited Au layer wets the substrate and hence prevents reactant molecules from interaction with the oxide support. (v) Stabilization by anchoring. The support

**Received:** May 7, 2013

**Revised:** July 17, 2013

**Published:** July 24, 2013



provides specific sites, e.g. defects, which facilitate nucleation, suppress cluster mobility, and prevent coalescence. Also, the number of low coordinated atoms is partially controlled by the support via the cluster density and shape.<sup>22</sup>

In the present work we study the adsorption of carbon monoxide and oxygen and their potential reaction on gold clusters grown on a completely different class of template in order to obtain new insights into the role of the support material. Recently, it has been shown that carburized W(110) surfaces serve as rather universal substrates for the growth of different kinds of noble-metal clusters:<sup>29–31</sup> The low carbon coverage R(15 × 12)C/W(110) phase is an excellent template for generation of regularly arranged monolayer-height clusters of a rather fixed size (ca. 7 atoms) (see Figure 3c), while on the high carbon coverage R(15 × 3)C/W(110) template bilayer particles with lateral extensions up to a few nanometers (depending on Au coverage) are generated (see Figure 3a). The proposed cluster/support system seems to be a promising candidate for investigation of the catalytic properties toward CO oxidation for several reasons: The substrate—a surface carbide—is metallic and hence differs from conventionally used insulating/semiconducting oxidic supports. Therefore, exploration of the adsorption behavior of oxygen and carbon monoxide as well as the reactivity toward oxidation is expected to yield interesting results concerning the role of the support material. Whereas arguments based on the abundant existence of undercoordinated gold sites or on quantum-size effects due to lateral electron confinement are valid on both insulating and metallic substrates, from other arguments such as charge transfer or reaction at the gold/support interface a different behavior is expected. Furthermore, use of carburized W(110) as template allows growth of well-defined clusters of both monolayer height (Au/R(15 × 12)) and bilayer height (Au/R(15 × 3)) on rather similar substrates. As already mentioned above, a thickness of two monolayers is regarded essential for the activity of Au nanocatalysts by some authors.<sup>10,13,17</sup> In addition—as gold clusters are reported to catalyze not only oxidation of carbon monoxide but also other oxidation reactions as well—the question will be addressed if the gold clusters are also able to catalyze oxidation of the carburized template itself.

In order to test the stability of the cluster systems in a gas atmosphere, in-situ room temperature STM measurements were performed for both reactants. Temperature-programmed desorption (TPD) experiments after low-temperature ( $\approx$ 90–100 K) adsorption of oxygen or carbon monoxide were carried out on the templates as well as on the cluster-decorated samples. Finally, coadsorption/reaction studies for investigation of the catalytic activity were performed.

## 2. EXPERIMENT

All experiments were carried out in an UHV chamber with a base pressure of  $2 \times 10^{-10}$  mbar, equipped with a room-temperature scanning tunneling microscope (Danish Micro Engineering) and a quadrupole mass filter (Inficon) for TPD measurements. High temperatures (1000–2600 K) required for sample cleaning and preparation of the carbon superstructures were achieved by electron bombardment; for TPD experiments the crystal was heated ohmically. Up to 1200 K (i.e., in TPD measurements) sample temperatures were measured with a type C (W-5% Re/W-26% Re) thermocouple spot-welded to a thin tantalum foil which was clamped to the tungsten sample. Because of temperature gradients across the Ta foil, at high

temperatures the temperature readout from the thermocouple resulted in too low values (by approximately 100–150 at 1200 K). Hence, beyond 1200 K (i.e., during sample preparation) a two-color pyrometer was used. Temperatures given in TPD spectra are always noncorrected thermocouple readings.

The surface was cleaned from carbon impurities by heating in oxygen as described in refs 30 and 32–34. Tungsten oxides formed in course of the procedure were removed by flashing the sample to 2300–2600 K. The carbon superstructures were generated following the preparation routines as described in refs 29, 30, 35, and 36. Carbon was provided by thermolysis of ethene ( $C_2H_4$ ) (heating for 10 min at 1250 K in  $5 \times 10^{-8}$  mbar). Subsequent annealing at 1250 K in vacuum led to broader terraces. Flashing to 1900 K produced sharp R(15 × 3) LEED spots, whereas either flashing to 2300 K or annealing for 2 min at 2000 K, both followed by rapid cooling, yielded the typical R(15 × 12) pattern.<sup>30</sup> Gold was evaporated from a resistively heated alumina crucible. The deposition flux was set by the heating power only. Accordingly, deposition rates in different experiments varied between 0.10 and 0.20 monolayers (ML) per minute, as estimated from STM images of extended gold islands generated on W(110). For the production of well-ordered regular arrays of gold monolayer clusters on R(15 × 12) the sample had to be kept at 600–700 K. In contrast, to achieve kinetically controlled growth of nanosized bilayer clusters (rather than growth of larger ribbon-like multilayer structures), gold deposition on R(15 × 3) had to be carried out at room temperature.

In-situ STM measurements were performed during gas exposure at room temperature, using gas pressures (either CO or  $O_2$ ) of  $5 \times 10^{-8}$  mbar. Gas exposures are specified in langmuirs (1 langmuir =  $10^{-6}$  Torr·s). Unless otherwise noted, for TPD experiments, the sample was kept at 90–100 K during adsorption and subsequently heated with rates of 5–8 K/s.

## 3. ADSORPTION OF CO ON CLEAN AND CARBURIZED W(110)

Figure 1 shows TPD spectra obtained after saturation CO exposure to clean W(110) as well as to the two carburized

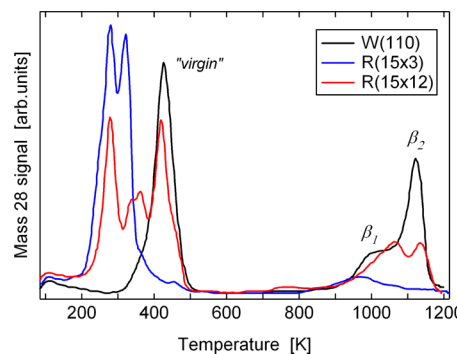


**Figure 1.** TPD spectra of CO on W(110), R(15 × 3)C/W(110), and R(15 × 12)C/W(110). CO exposures are 5.9, 11.5, and 11.5 langmuirs, respectively.

surface phases. The evolution of the various peaks as a function of CO exposure is displayed in the Supporting Information, Figures S1–S3. The spectra taken on clean W(110) are in agreement with literature data,<sup>37–39</sup> showing the low-temperature “virgin” peak slightly above 400 K and the high-temperature double-peak feature (“ $\beta$ ”) at 1000–1100 K.

Whereas the virgin peak stems from molecularly adsorbed carbon monoxide, the high-temperature  $\beta$  features are commonly attributed to CO molecules adsorbed dissociatively on W(110),<sup>38,40,41</sup> although Lee and co-workers recently doubted if CO molecules are completely dissociated or only strongly tilted.<sup>42</sup> However, our TPD data after oxygen adsorption on the carburized templates strongly support the dissociation model (see section 5).

The TPD data for CO adsorbed on the R( $15 \times 3$ ) carbon superstructure differ from that of the clean surface in several respects: (i) The low-temperature feature is split into two components, suggesting a coverage-dependent adsorption energy and/or the existence of (at least) two different adsorption sites. The latter interpretation seems plausible due to the heterogeneous character of the R( $15 \times 3$ ) surface (consisting of C and W atoms) and the fairly large size of the unit cell (having a size equivalent to 15 tungsten surface atoms). The surface is therefore likely to offer different adsorption sites. (ii) The (split) low-temperature feature is shifted to lower desorption temperatures, indicating a weakened adsorption of molecular CO on carbon-modified tungsten. (iii) The high-temperature  $\beta$  features have practically disappeared. If the  $\beta$  features arise from dissociated CO, an obvious explanation for their suppression is the blocking of adsorption sites for atomic carbon, since the R( $15 \times 3$ ) surface is already presaturated with carbon. An alternative explanation would be a substantial C-induced increase of the activation barrier for CO dissociation.

The TPD spectra from the low carbon-coverage R( $15 \times 12$ ) surface exhibit a more complicated pattern (see Figure 1) with (at least) six components: four at low temperatures (280–420 K) and two at high temperatures (1050–1150 K). We interpret the existence of the pronounced 420 K peak as well as the high-temperature double feature (which all exhibit peak temperatures similar to clean tungsten) as an indication of CO adsorption on sites that are only weakly perturbed by the presence of carbon. As we have shown recently, the W(110) surface is not uniformly covered with R( $15 \times 12$ ): Wide terraces, exhibiting the R( $15 \times 12$ ) structure, coexist with smaller terraces being essentially free of carbon.<sup>29</sup> Furthermore, STM images of the large R( $15 \times 12$ ) unit cell (having a size equivalent to 60 tungsten surface atoms) exhibit “bright” regions, which were interpreted as being largely free of carbon atoms.<sup>43</sup>

The three low-temperature features (370 K and below) are attributed to CO molecules adsorbed in parts of the R( $15 \times 12$ ) unit cell, where CO is more strongly influenced by carbon atoms from the template, resulting in desorption temperatures rather similar to that from the high carbon coverage R( $15 \times 3$ ) phase.

The uptake curves (at 90 K) for CO on the three templates as derived from the integrated TDS intensities are summarized in Figure 2. All curves are quite similar, showing a precursor-mediated adsorption behavior with a linear coverage increase for exposures up to 3.4 langmuirs and an almost constant coverage for larger exposures. The achievable saturation coverages on both carburized surfaces are roughly equal to that on clean W(110), for which saturation values between 0.7 and 1.1 ML were derived in the literature.<sup>44–46</sup> In good agreement with these values, we calculate a saturation coverage of 0.9 ML from the required saturation exposure of 3.4 langmuirs under the assumption of a constant unity sticking coefficient.

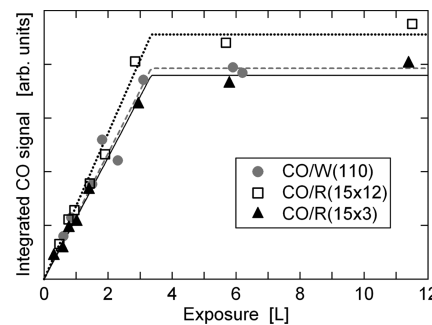


**Figure 2.** CO uptake curves (at 90 K) on W(110), R( $15 \times 12$ )C/W(110), and R( $15 \times 3$ )/C/W(110) as obtained from the integrated TPD curves.

The present TPD measurements of CO adsorption on R( $15 \times 3$ ) are similar to TPD data of CO adsorption on C/W(111) and C/W(110) by Hwu et al.,<sup>47,48</sup> both showing a double-peak desorption structure around 300 K and a strong reduction of the high-temperature desorption feature stemming from dissociated CO. In Hwu’s work on C/W(110) an ordered C-induced LEED pattern was not observed, probably due to the relatively low flash preparation temperature of 1200 K. However, from the preparation procedure used and the amount of carbon detected by AES, we conclude that the surface should be carbon-rich and hence similar to our ordered R( $15 \times 3$ ) phase.

Analogous to the present findings, measurements on C/W(100) revealed that with increasing carbon content of the surface the ability to dissociate CO is reduced, while the overall amount of adsorbed CO is always roughly the same.<sup>49</sup>

It is also quite instructive to compare the adsorption properties of the carburized tungsten surfaces with those of tungsten carbide single crystals. Freund and co-workers investigated the interaction of CO with a “stoichiometric” WC(0001) surface and found that CO adsorbs molecularly below room temperature.<sup>50</sup> Around 250 K CO desorbs partly, while the remaining CO dissociates. This behavior is qualitatively similar to that of clean W(110) or R( $15 \times 12$ )C/W(110) but clearly differs from that observed for the high-carbon coverage R( $15 \times 3$ ) phase, where dissociation of CO is effectively suppressed. According to the structural studies of the same group, tungsten carbide (which is a layered hexagonal crystal) terminates with a tungsten surface layer, on which about 30% of carbon atoms are statistically distributed.<sup>51</sup> This would explain the close similarity to the clean W(110) and the low-carbon-coverage R( $15 \times 12$ ) surface, while the carbon-saturated R( $15 \times 3$ ) surface behaves differently.

#### 4. ADSORPTION OF CO ON AU-DECORATED CARBURIZED W(110)

In Figure 3, the results of an in-situ STM study of the influence of CO on Au clusters on R( $15 \times 3$ )C/W(110) and R( $15 \times 12$ )C/W(110), respectively, are displayed. As clearly seen from the images, both types of nanoparticles are stable under CO exposure at room temperature, irrespective of the type of C/W(110) substrate. Furthermore, due to the low Au coverage on R( $15 \times 3$ ), the STM images also demonstrate that the substrate itself—visible as faint, protruding lines with an intrinsic height of 0.8 nm—is unaffected by CO at room temperature. This might have been expected, since CO already desorbs around

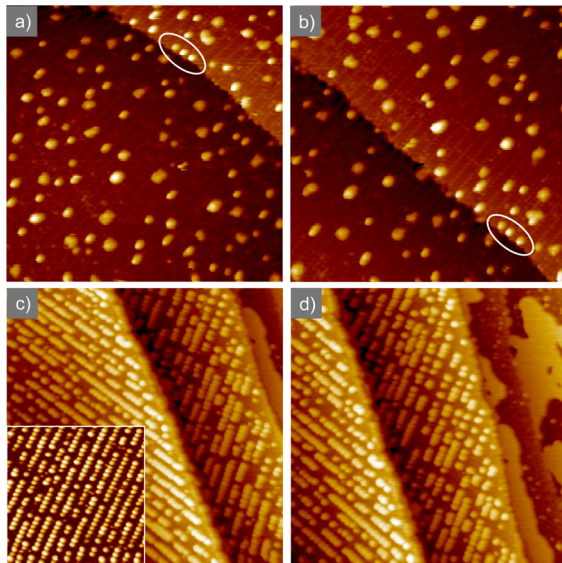


**Figure 3.** STM images of Au clusters on R( $15 \times 3$ )C/W(110) (top) as well as R( $15 \times 12$ )C/W(110) (bottom) before (left) and after (right) exposure to CO (b: 75 langmuirs, d: 181 langmuirs). Au coverages: (a, b) 0.5 min; (c, d) 1.5 min. Image sizes: (a, b) 40 nm  $\times$  40 nm; (c, d) 80 nm  $\times$  80 nm. Note the growth of extended gold islands on the narrow carbon-poor tungsten terraces, visible on the right-hand side of images c and d. The better resolved inset in (c) shows that the line-like structures visible in (c) and (d) actually consist of individual small gold clusters.

room temperature from the R( $15 \times 3$ ) surface (compare Figure 1).

Deposition of Au on R( $15 \times 3$ ) essentially quenches the low-temperature “molecular” CO desorption features located at  $T \lesssim 400$  K (see Figure 4). This can be understood as a site-blocking

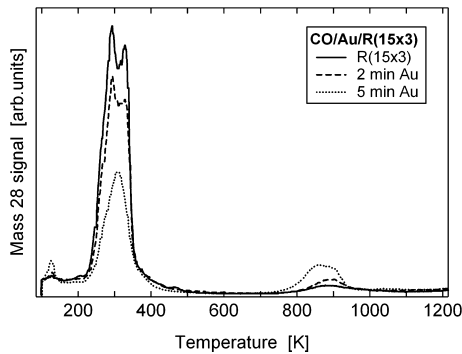


**Figure 4.** TPD spectra of Au/R( $15 \times 3$ )C/W(110) after exposure to 10 langmuirs of CO. A deposition time of 1 min corresponds to a coverage of 0.1–0.2 ML.

effect. Surprisingly, at high temperatures (ca. 850–900 K) a new CO desorption feature evolves with increasing gold coverage. It is tempting to attribute this observation to CO molecules adsorbed at the periphery or on top of the deposited gold particles. However, in view of the weak CO–gold interaction,<sup>52–56</sup> such a high desorption temperature seems to be impossible for molecularly adsorbed CO. It appears to be more reasonable to assign this desorption feature to recombinatively desorbing CO. This implies the presence of atomic oxygen which can only arise from CO dissociation. The

microscopic origin for this surprising Au-induced CO dissociation is unclear at present.

Finally, we turn to the low-temperature behavior, which is of crucial importance for a potential CO oxidation reaction. Various other groups who carried out adsorption studies on either Au surfaces<sup>52–56</sup> or Au nanoparticles<sup>55,16,56–58</sup> mostly found two CO desorption peaks at temperatures around  $\approx 120$  and  $\approx 190$  K, respectively. These peaks were frequently assigned to differently coordinated CO molecules (depending on author either as surface vs step or as step vs kink adsorption). Clearly, except for a marginal intensity increase at  $\approx 120$  K, Au-induced low-temperature features cannot be detected in this temperature regime. In the work of Freund and co-workers, CO desorption temperatures up to 300 K were reported for as-deposited, unannealed small Au particles and attributed to CO molecules attached to highly uncoordinated Au atoms.<sup>16,58</sup> It might well be that due to the small size of the Au particles in the present study a similar desorption feature is hidden underneath the template-induced double-peak desorption feature at temperatures around 250–300 K. However, according to Freund et al., this “hidden” peak should shift to lower temperatures with increasing particle size (i.e., coverage) and hence become visible as an extra feature in the TDS spectra. As this behavior is not observed, we conclude that the Au clusters on R( $15 \times 3$ )C/W(110) are not—or only marginally—able to adsorb weakly bound CO molecules. Thus, our data parallel the findings of Outka and Madix that CO does not adsorb on Au(110) down to temperatures of 125 K.<sup>59</sup> As pointed out by these authors, this does not necessarily imply that CO does not stick on the surface. The residence time of CO on gold could just be too low to allow buildup of sufficient amounts of CO that could be detected by TDS. Furthermore, in the present case CO attaching to the gold clusters could also spill over to the substrate or the gold/substrate interface, where it is more strongly bound.

CO TPD spectra with different amounts of Au on R( $15 \times 12$ )C/W(110) are displayed in Figure 5. Deposition of gold

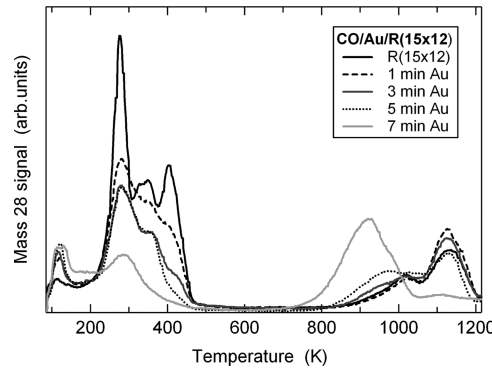


**Figure 5.** TPD spectra of Au/R( $15 \times 12$ )C/W(110) after exposure to 10 langmuirs of CO. Gold deposition rate was 0.1–0.2 ML/min.

leads to an intensity decrease of the desorption features in the temperature region from 300 to 420 K due to blocking of CO adsorption sites. The 420 K peak, resulting from CO molecules only weakly affected by the presence of carbon, is reduced most strongly, indicating preferential Au nucleation in these surface regions. Our STM findings concerning the growth behavior of Au<sup>36</sup> corroborate this assumption: Preferentially, Au nucleates on carbon-poor regions of the unit cell; at elevated deposition temperatures (i.e., 700 K) Au atoms in “excess” of the optimum

coverage ( $\approx 0.12$  ML) diffuse to W(110) terraces always coexisting with the broader carbon-modified ones.<sup>29,36</sup> Hence, tungsten-rich areas on the surface (clean terraces as well as carbon-poor regions within the unit cell) are preferentially covered with Au atoms—leading to a selective decrease of the signal attributed to CO desorption from these areas.

The high-temperature  $\beta$  features do not follow this behavior but (for deposition times up to 5 min) remain rather unaffected in position and peak intensity. However, one should mention that at such high temperatures (around 1000 K) the gold clusters do no longer retain their room temperature size and shape. STM investigations performed after flashing the small clusters of Figure 3c to  $\approx 1000$  K showed rectangular-shaped clusters with heights beyond one monolayer and lateral extensions up to several nanometers. Interestingly, for gold deposition times exceeding 5 min the high-temperature desorption feature changes its appearance drastically: The peak at  $\approx 1100$  K is quenched almost completely; instead, a strong new peak appears around 900 K. We presume that this change is again related with a structural change. A possible scenario would be that under the presence of sufficient amounts of gold the underlying R( $15 \times 12$ ) template is altered. A different explanation—not necessarily in contradiction to the former one—is related to a change in growth behavior at “higher” gold coverages. As is known from our previous studies of the analogous Ag/R( $15 \times 12$ ) system,<sup>29</sup> atoms deposited in excess of the ideal coverage of the cluster structure ( $\approx 0.12$  ML) mostly diffuse to nearby clean tungsten terraces, where they form extended islands. However, at some stage the Ag atoms start to fill the space between the clusters and to overgrow them as larger bilayer islands. Accordingly, we suppose that the evolution of the strong 900 K peak is associated with the formation of double-layer high gold islands. This explanation is consistent with the TPD experiments on the R( $15 \times 3$ ) substrate (Figure 4): On this surface bilayer islands are formed already at low Au coverages. Accordingly, the 900 K peak evolves (without “delay”) already at small gold coverages. STM investigations of CO-covered annealed surfaces with various Au precoverages are necessary to clarify this issue.

As already observed for the R( $15 \times 3$ ) template in the low-temperature region below 300 K pronounced Au-induced features do not appear except for a weak desorption signal at  $\approx 120$  K. However, since in the series of experiments the desorption intensity at 120 K (i.e., close to the adsorption temperature) could not be reproduced perfectly, the assignment of the intensity increase as a Au-induced effect is not unambiguous. In any case, the desorption signal at 120 K is comparatively small. This indicates that weakly adsorbed CO is only present in small amounts—if at all—on the Au clusters on the R( $15 \times 12$ ) template, which parallels the findings for R( $15 \times 3$ ). Lower adsorption temperatures or much higher CO pressures would be needed. From these results we can already guess that low-temperature CO oxidation on both types of Au clusters is unlikely with the present systems.

## 5. ADSORPTION OF OXYGEN

The stability of both carburized templates with and without Au clusters against exposure to oxygen atmosphere was investigated by STM “movies” at room temperature as well as by temperature-programmed desorption experiments after adsorption at 90–100 K.

STM experiments on the bare templates showed a rather good stability for both R( $15 \times 3$ ) and R( $15 \times 12$ ). Although

the images were somewhat deteriorated (possibly due to tip instabilities in the presence of oxygen) and although in particular on the R( $15 \times 3$ ) surface occasional impurities and hole-like defects appeared with prolonged gas exposure and scanning time, the overall periodicities seemed to be conserved.

The evolution of the Au-covered R( $15 \times 3$ )C/W(110) surface upon O<sub>2</sub> exposure is shown in Figure 6a,b. (More

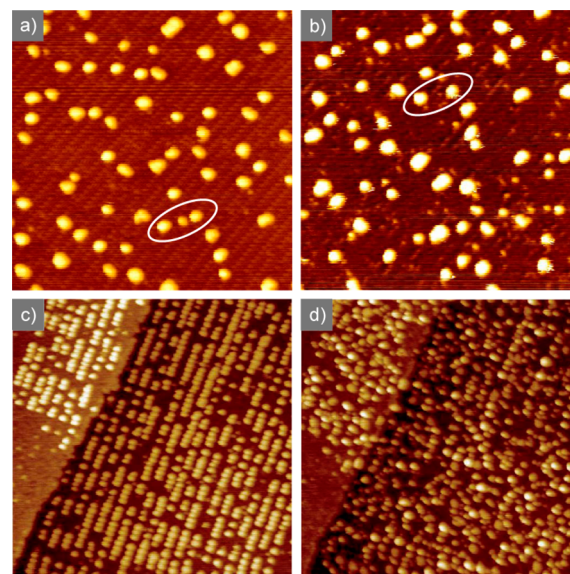


**Figure 6.** In-situ STM study of the influence of oxygen ( $p = 5 \times 10^{-8}$  mbar) on the R( $15 \times 3$ ) and R( $15 \times 12$ ) templates covered with Au clusters: (a) R( $15 \times 3$ ), before gas exposure, (b) R( $15 \times 3$ ) after 55 langmuirs of O<sub>2</sub>, (c) R( $15 \times 12$ ), before gas exposure, (d) R( $15 \times 12$ ) after 86 langmuirs of O<sub>2</sub>. Image sizes: 40 nm  $\times$  40 nm (a, b) and 80  $\times$  80 nm (c, d).

images are shown in the Supporting Information, Figures S4 and S5.) Apart from very occasional modifications (such as the disappearing cluster in the center of the white marker) the bilayer gold particles obviously are quite stable to O<sub>2</sub>. By contrast, pronounced oxygen-induced changes occur for the Au clusters on the R( $15 \times 12$ ) template (see Figure 6c,d). With increasing oxygen exposure the originally well-aligned nanodots show strong modifications: Increasing oxygen exposure leads to less perfect ordering, the size distribution is broadened significantly, and some bilayer clusters are formed. After an exposure of  $\approx 90$  langmuirs a quite stable state is reached; the clusters are hardly altered anymore. Agglomeration to larger islands, supposedly exhibiting a negative effect on the reactivity of Au clusters, is not observed. Note that the rather strong oxygen-induced alterations of the gold nanoparticles indicate dissociation of the oxygen molecules on or at least in close vicinity of the Au clusters on the R( $15 \times 12$ ) substrate.

TPD experiments performed after oxygen exposure of both the bare and the Au-covered carburized templates never revealed an O<sub>2</sub> desorption signal. Instead, only desorption of CO was observed as shown in Figures 7 and 8.

The CO desorption spectrum from the bare R( $15 \times 12$ ) surface (Figure 7) bears a close resemblance to the high-temperature  $\beta$  features observed for CO desorption (after CO exposure) from clean W(110) as shown in Figure 1. Obviously, oxygen molecules dissociate on the surface and react with carbon atoms from the templates: CO is formed and desorbs at high temperatures (900–1100 K). These temperatures are

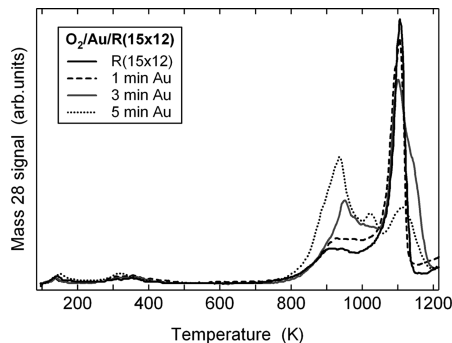


**Figure 7.** CO desorption spectra of bare and Au-covered R( $15 \times 12$ ) after exposure to 10 langmuirs of oxygen. Gold deposition rate was 0.1–0.2 ML/min.

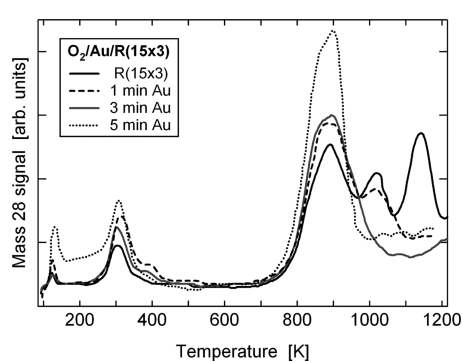


**Figure 8.** CO desorption spectra of bare and gold-covered R( $15 \times 3$ ) after exposure to 10 langmuirs of CO. Gold deposition rate was 0.1–0.2 ML/min.

rather similar to that of dissociated  $\beta$ -CO on clean W(110), thus lending strong support to the interpretation of the  $\beta$  desorption peaks as stemming from dissociated CO. This observation is in accordance with the findings of Viswanath and Schmidt that the desorption properties for oxygen and carbon on W(100) “are essentially identical to those of adsorbed carbon monoxide”.<sup>60</sup> Addition of gold decreases the intensity of the  $\beta_2$ -like peak at 1100 K but increases the intensity of the  $\beta_1$ -like feature around 950 K. Hence, the presence of Au shifts the maximum in the desorption rate by approximately 150 K toward lower temperatures, implying that gold obviously catalyzes the associative reaction of surface carbon with adsorbed oxygen to gaseous carbon monoxide. According to the principle of detailed balance, then the reverse process of dissociative CO adsorption should also be catalyzed—in agreement with our findings concerning CO adsorption in the presence of gold clusters.

A similar effect is seen on the R( $15 \times 3$ ) template (Figure 8). Here, the desorption rate at 900 K increases markedly when gold is present on the surface, while the higher-temperature peaks are reduced in intensity. Surprisingly, on both bare and Au-covered R( $15 \times 3$ ) some CO formation and desorption occur even around room temperature. Tentatively, we assign this feature to carbon atoms in excess of the amount required to form an ideal R( $15 \times 3$ ) structure, which can be more easily oxidized. The increased desorption signal at even lower temperatures as (reproducibly) observed with larger amounts of gold (5 min) also remains without definite explanation. In contrast, the finite desorption signal at and even above 1200 K can be traced back to the onset of segregation and subsequent

oxidation of carbon atoms residing in subsurface regions of the R( $15 \times 3$ ) phase.

In summary, the TPD investigations show that oxygen molecules dissociate on both carburized tungsten surfaces. CO is formed, and this reaction is promoted by the presence of gold. The STM investigation on the R( $15 \times 12$ ) surface even prove that oxygen atoms reside at or in close vicinity to the Au clusters. However, “weakly” bound oxygen atoms which recombine and desorb at intermediate temperatures (around 500 K)—as found e.g. on Au(110), see ref 61—were not observed. We conclude that either oxygen dissociates only at the template itself or that—even if oxygen dissociates on or in close vicinity to the Au nanoparticles—it subsequently spills over to the C/W(110) substrate, where it reacts with the surface carbon and desorbs as CO. The modifications of the Au clusters induced by exposure to O<sub>2</sub> as seen by STM could then be explained by a displacement of Au atoms due to the competitive adsorption of dissociated oxygen for (the same) favorable adsorption sites. Because of the large binding energy of oxygen to tungsten (adsorption energy 4.20 eV/atom<sup>62</sup>), we expect that the carbon-poor regions where the Au clusters nucleate are also the most favorable areas for oxygen adsorption, thus providing a strong driving force for an oxygen-induced rearrangement of the noble-metal clusters. However, as the oxygen atoms on W(110) are bound rather strongly to the surface, we expect that they are not available for the low-temperature formation of CO<sub>2</sub>, leading to the conclusion that also for this reason the system—despite its ability to dissociate molecular oxygen—will not be able to perform CO combustion.

## 6. REACTION STUDIES AND CONCLUSIONS

CO oxidation studies were performed, looking for CO<sub>2</sub> formation in temperature-programmed reaction experiments under various reaction conditions: (i) alternating chronological order of exposures, (ii) low ( $5 \times 10^{-8}$  mbar) and “high” ( $1 \times 10^{-6}$  mbar) total “steady-state” background pressures, (iii) different O<sub>2</sub>/CO ratios (1:1 or oxygen surplus in order to avoid blocking of reactive sites by CO), and (iv) utilizing linear as well as stepwise temperature profiles (both starting at 90 K). Furthermore, preadsorption of oxygen at 300 K, followed by heating in CO atmosphere (starting at 90 K), was also tested, as STM on the R( $15 \times 12$ ) revealed that at 300 K oxygen adsorbs dissociatively on or close to the Au clusters. However, in none of these experiments could the evolution of CO<sub>2</sub> due to Au-catalyzed CO oxidation be verified, neither for bilayer clusters on the R( $15 \times 3$ ) nor for the small monolayer clusters on the R( $15 \times 12$ ) template, although the gain of the QMS was increased up to 100-fold compared to the CO and O<sub>2</sub> TPD experiments. Hence, we conclude that in the systems investigated in the present work CO oxidation is not possible, at least not under the present experimental low-pressure conditions.

The TPD experiments presented in sections 4 and 5 provide a reasonable explanation for this observation: neither weakly bound carbon monoxide molecules nor oxygen atoms attached to gold clusters, with desorption temperatures below 200 K (CO) or around 500 K (oxygen), respectively, could be observed. Although CO oxidation turned out to be unsuccessful, several conclusions on the catalytic activity of Au nanoparticles can be drawn from our adsorption/desorption experiments:

1. The clusters used in the present study were of similar size (ranging from  $\approx$ 7 atoms to diameters of a few nanometers) as in related studies, where CO combustion could be successfully performed (see for example refs 4–6 and references therein). Furthermore, clusters of monolayer as well as bilayer height were used, with the latter thickness reported to be particularly active for CO oxidation.<sup>10,13,17</sup> Despite these structural similarities, different CO and oxygen adsorption properties were measured. Hence, the present study shows that tailoring intrinsic cluster properties, such as small size, high number of undercoordinated Au atoms, or suitable thickness (2 ML), does not suffice to obtain the adsorption behavior required for CO oxidation. Obviously, the function of the support is not only to provide suitable nucleation sites for generation of well-shaped and anchored Au nanoparticles, but in contrast the support has to actively influence the adsorption properties and in turn the catalytic activity.

2. Commonly, dissociation of oxygen is considered as the main obstacle in CO oxidation. However, with the present material combinations definite evidence for weakly adsorbed CO on the gold clusters could not be found. Obviously, for the present systems also the CO adsorption/desorption behavior might limit the oxidation reaction. As in the present system, CO obviously desorbs already below 100 K from the Au clusters; this would require much higher CO pressures for successful  $\text{CO}_2$  formation than in other more “usual” systems.

3. In all investigated systems dissociation of oxygen occurred but not necessarily always at the Au clusters. However, at least for monolayer Au clusters on R(15  $\times$  12)C/W(110) the STM images provide strong evidence for oxygen dissociation on or in the immediate vicinity of the Au clusters. As an  $\text{O}_2$  desorption feature characteristic for dissociated oxygen on gold is not observed, we conclude that even if  $\text{O}_2$  is dissociated at Au clusters, the dissociated oxygen atoms spill over to the template, where they are bound strongly and thus are not available for low-temperature reactions. Hence, even if adsorption of CO on the Au clusters was possible, the strong affinity between oxygen atoms and the support would probably lead to a suppression of the catalytic activity. In such a case the substrate actually poisons the desired oxidation reaction. Put into more general terms: Reductive materials as the presently used C/W templates are not suitable as supports for Au-catalyzed CO oxidation. Hence, we suppose that in order to achieve CO oxidation with the present supports, they first have to be heavily oxidized before the final reaction can take place.

The in-situ STM investigations revealed considerable differences between mono- and bilayer clusters on C/W(110), indicating oxygen-induced “corrosion” of the small monolayer-height clusters but not of the larger bilayer particles. Nevertheless, TDS and TPR studies did not feature strong distinctions between both cluster types. Hence, it might also be possible that in both cases oxygen molecules dissociate at the gold clusters, from where the oxygen atoms migrate to the support. We attribute the different stability of the Au clusters on the R(15  $\times$  12) and the R(15  $\times$  3) phases to the presence of carbon-poor, clean-tungsten-like adsorption sites underneath the Au clusters on the R(15  $\times$  12) surface. As mentioned above, these clean-tungsten-like areas are also favorable adsorption sites for oxygen, leading to a partial displacement of the gold particles on R(15  $\times$  12). We note that similar oxygen-induced displacement reactions were also observed for silver islands on clean W(110).<sup>63</sup> On the carbon-saturated R(15  $\times$  3) template such clean-tungsten-like regions are not available.

Accordingly, the driving force for restructuring the gold particles is missing, and the gold clusters remain unaltered. To some extent this parallels electrochemical measurements on WC and  $\text{W}_2\text{C}$  films, which show that the carbon-poor  $\text{W}_2\text{C}$  is readily oxidized to tungsten oxide, whereas the carbon-richer WC film is stable to higher anode potentials.<sup>64</sup>

In contrast to low-temperature CO oxidation, which is not possible under our experimental conditions, our study reveals a promoting effect of the deposited gold particles for the high-temperature oxidation of the carburized surfaces toward CO. On both templates associative CO formation at around 900 K is enhanced by gold, whereas the CO desorption features around  $\approx$ 1100 K are reduced in intensity. In agreement with that, dissociative CO adsorption as the reverse process is also catalyzed by the presence of gold. While on R(15  $\times$  3) this effect can already be observed for small submonolayer gold coverages, on R(15  $\times$  12) larger coverages are required. A tentative explanation for this delayed onset is related to the formation of bilayer Au clusters which form already at smallest gold coverages on R(15  $\times$  3) but only at elevated coverages (roughly around 0.5–1 ML) on R(15  $\times$  12).

## ■ ASSOCIATED CONTENT

### § Supporting Information

TPD series after different CO exposures to W(110), R(15  $\times$  3)C/W(110), and R(15  $\times$  12)C/W(110) (Figures S1–S3); more in-situ STM images acquired during  $\text{O}_2$  exposure to Au/R(15  $\times$  3) and Au/R(15  $\times$  12) (Figures S4 and S5). This material is available free of charge via the Internet at <http://pubs.acs.org>.

## ■ AUTHOR INFORMATION

### Corresponding Author

\*E-mail norbert.memmel@uibk.ac.at, Ph +43-512-507 5073, Fax +43-512-5007 2925 (N.M.).

### Notes

The authors declare no competing financial interest.

<sup>§</sup>Recipient of a Doc-fForte fellowship of the Austrian Academy of Sciences.

## ■ ACKNOWLEDGMENTS

Financial support of the work through the Austrian science fund (grant S9004-N20) and the Austrian Academy of Sciences (Doc-fForte fellowship for M. Bachmann) is gratefully acknowledged. We thank B. Klötzer for stimulating discussions and R. Pramsoler for excellent and in-time technical assistance.

## ■ REFERENCES

- (1) Haruta, M.; Kobayashi, T.; Sano, H.; Yamada, N. Novel Gold Catalysts for the Oxidation of Carbon Monoxide at a Temperature Far Below 0°C. *Chem. Lett.* **1987**, *16*, 405–408.
- (2) Takei, T.; Akita, T.; Nakamura, I.; Fujitani, T.; Okumura, M.; Okazaki, K.; Huang, J.; Ishida, T.; Haruta, M. Heterogeneous Catalysis by Gold. *Adv. Catal.* **2012**, *55*, 1–126.
- (3) Heiz, U.; Bullock, E. L. Fundamental Aspects of Catalysis on Supported Metal Clusters. *J. Mater. Chem.* **2004**, *14*, 564–577.
- (4) Meyer, R.; Lemire, C.; Shaikhutdinov, S.; Freund, H. J. Surface Chemistry of Catalysis by Gold. *Gold Bull.* **2004**, *37*, 72–124.
- (5) Min, B. K.; Friend, C. M. Heterogeneous Gold-Based Catalysis for Green Chemistry: Low-Temperature CO Oxidation and Propene Oxidation. *Chem. Rev.* **2007**, *107*, 2709.
- (6) Kung, M. C.; Davis, R. J.; Kung, H. H. Understanding Au-Catalyzed Low-Temperature CO oxidation. *J. Phys. Chem. C* **2007**, *111*, 11767–11775.

- (7) Bond, G. C.; Thompson, D.T. Gold-Catalysed Oxidation of Carbon Monoxide. *Gold Bull.* **2000**, *33*, 41–51.
- (8) Hutchings, G. New Directions in Gold Catalysis. *Gold Bull.* **1996**, *37*, 3–11.
- (9) Valden, M.; Lai, X.; Goodman, D. W. Onset of Catalytic Activity of Gold Clusters on Titania with the Appearance of Nonmetallic Properties. *Science* **1998**, *281*, 1647.
- (10) Chen, M. S.; Goodman, D. W. The Structure of Catalytically Active Gold on Titania. *Science* **2004**, *306*, 252.
- (11) Green, I. X.; Tang, W.; Neurock, M.; Yates, J. T. Spectroscopic Observation of Dual Catalytic Sites during Oxidation of CO on a Au/TiO<sub>2</sub> Catalyst. *Science* **2011**, *333*, 736–739.
- (12) Remediakis, I. N.; Lopez, N.; Nørskov, J. K. CO Oxidation on Rutile-Supported Au Nanoparticles. *Angew. Chem., Int. Ed.* **2005**, *44*, 1824–1826.
- (13) Chen, M. S.; Goodman, D. W. Structure-Activity Relationships in Supported Au Catalysts. *Catal. Today* **2006**, *11*, 22–33.
- (14) Yoon, B.; Häkkinen, H.; Landman, U.; Wörz, A. S.; Antonietti, J. M.; Abbet, S.; Judai, K.; Heiz, U. Charging Effects on Bonding and Catalyzed Oxidation of CO on Au<sub>8</sub> Clusters on MgO. *Science* **2005**, *307*, 403–407.
- (15) Lemire, C.; Meyer, R.; Shaikhutdinov, S.; Freund, H.-J. Do Quantum-Size Effects Control CO Adsorption on Gold Nanoparticles? *Angew. Chem., Int. Ed.* **2004**, *43*, 118–121.
- (16) Lemire, C.; Meyer, R.; Shaikhutdinov, S.; Freund, H.-J. CO Adsorption on Oxide-Supported Gold: From Small Clusters to Monolayer Islands and Three-Dimensional Nanoparticles. *Surf. Sci.* **2004**, *552*, 27–34.
- (17) Herzing, A. A.; Kiely, C. J.; Carley, A. F.; Landon, P.; Hutchings, G. J. Identification of Active Gold Nanoclusters on Iron Oxide Supports for CO Oxidation. *Science* **2008**, *321*, 1331–1335.
- (18) Turner, M.; Golovko, V. B.; Vaughn, O. P. H.; Abdulkin, P.; Berenguer-Murcia, A.; Tikhov, M. S.; Johnson, B. F. G.; Lambert, R. M. Selective Oxidation with Dioxygen by Gold Nanoparticle Catalysts Derived from 55-Atom Clusters. *Nature* **2008**, *454*, 981–984.
- (19) Guczi, L.; Petö, G.; Beck, A.; Frey, K.; Geszti, O.; Molnár, G.; Daróczy, C. Gold Nanoparticles Deposited on SiO<sub>2</sub>/Si(100): Correlation Between Size, Electron Structure, and Activity in CO Oxidation. *J. Am. Chem. Soc.* **2002**, *125*, 4332–4337.
- (20) Falsig, H.; Hvoelbæk, B.; Kristensen, I. S.; Jiang, T.; Bligaard, T.; Christensen, C. H.; Nørskov, J. K. Trends in the Catalytic CO Oxidation Activity of Nanoparticles. *Angew. Chem., Int. Ed.* **2008**, *47*, 4835–4839.
- (21) Roldán, A.; Novell, G.; Ricart, J. M.; Illas, F. Theoretical Simulation of Temperature-Programmed Desorption of Molecular Oxygen on Isolated Au Nanoparticles from Density Functional Calculations and Microkinetic Models. *J. Phys. Chem. C* **2010**, *114*, 5101–5106.
- (22) Comotti, M.; Li, W.-E.; Spliethoff, B.; Schüth, F. Support Effect in High Activity Gold Catalysts for CO Oxidation. *J. Am. Chem. Soc.* **2006**, *128*, 917–924.
- (23) Fu, L.; Wu, N. Q.; Yang, J. H.; Qu, F.; Johnson, D. L.; Kung, M. C.; Kung, H. H.; Dravid, V. P. Direct Evidence of Oxidized Gold on Supported Gold Catalysts. *J. Phys. Chem. B* **2005**, *109*, 3704–3706.
- (24) Casaleotto, M. P.; Longo, A.; Martorana, A.; Prestianni, A.; Venezia, A. M. XPS Study of Supported Gold Catalysts: The Role of Au<sup>0</sup> and Au<sup>+δ</sup> Species as Active Sites. *Surf. Interface Anal.* **2006**, *38*, 215–218.
- (25) Minico, S.; Scire, S.; Crisafulli, C.; Visco, A. M.; Galvagno, S. FT-IR Study of Au/Fe<sub>2</sub>O<sub>3</sub> Catalysts for CO Oxidation at Low Temperature. *Catal. Lett.* **1997**, *47*, 273–276.
- (26) Fierro-Gonzalez, J. C.; Guzman, J.; Gates, B. C. Role of Cationic Gold in Supported CO Oxidation Catalysts. *Top. Catal.* **2007**, *44*, 103–114.
- (27) Haruta, M.; Daté, M. Advances in the Catalysis of Au Nanoparticles. *Appl. Catal., A* **2001**, *222*, 427–437.
- (28) Iizuka, Y.; Tode, T.; Takao, T.; Yatsu, K.; Takeuchi, T.; Tsubota, S.; Haruta, M. A. Kinetic and Adsorption Study of CO Oxidation Over Unsupported Fine Gold Powder and Over Gold Supported on Titanium Dioxide. *J. Catal.* **1999**, *187*, 50–58.
- (29) Bachmann, M.; Gabl, M.; Deisl, C.; Memmel, N.; Bertel, E. Quasi-One-Dimensional Self-Assembly of Metal Nanoclusters on C/W(110). *Phys. Rev. B* **2008**, *78*, 235410.
- (30) Bachmann, M.; Memmel, N.; Bertel, E.; Denk, M.; Hohage, M.; Zeppenfeld, P. Monitoring Preparation and Phase Transitions of Carburized W(110) by Reflectance Difference Spectroscopy. *Appl. Surf. Sci.* **2012**, *258*, 10123–10127.
- (31) Varykhalov, A.; Rader, O.; Gudat, W. Origin of Au Nanostructures on Tungsten Surface Carbides. *Phys. Rev. B* **2008**, *77*, 035412.
- (32) Stern, R. M. Tungsten (110) Surface Characteristics in Low-Energy Electron Diffraction. *Appl. Phys. Lett.* **1964**, *5*, 218–220.
- (33) Bauer, E. Multiple Scattering Versus Superstructures in Low-Energy Electron Diffraction. *Surf. Sci.* **1967**, *7*, 351–364.
- (34) Baudoing, R.; Stern, R. M. Metastable Surface Structure of the W(110) Face. *Surf. Sci.* **1968**, *10*, 392–398.
- (35) Gabl, M.; Bachmann, M.; Memmel, N.; Bertel, E. Interactions between Ag Nanoclusters on Carburized W(110). *Phys. Rev. B* **2009**, *79*, 153409.
- (36) Bachmann, M.; Memmel, N.; Bertel, E. Noble-Metal Nanostructures on Carburized W(110). *Surf. Sci.* **2011**, *605*, 1263–1270.
- (37) Kohrt, C.; Gomer, R. The Adsorption of CO on the (110) Plane of Tungsten. *Surf. Sci.* **1971**, *24*, 77–103.
- (38) Anders, L. W.; Hansen, R. S. Mixed Adsorption of Carbon Monoxide and Oxygen on Tungsten (100), (110), and (111) Single Crystal Faces. *J. Chem. Phys.* **1975**, *62*, 4652–4660.
- (39) Yang, T.; Jee, H.; Boo, J.; Han, H.; Lee, G.; Kim, Y.; Lee, S. Adsorption and Desorption of CO on W(110) Surfaces. *Bull. Korean Chem. Soc.* **2008**, *29*, 1115–1120.
- (40) Goymour, C. G.; King, D. A. Coadsorption of Oxygen and Carbon Monoxide on Tungsten: Desorption Spectra, Electron-Stimulated Desorption and Field Emission Microscopy. *Surf. Sci.* **1973**, *35*, 246–270.
- (41) Umbach, E.; Fugle, J. C.; Menzel, D. Adsorbate Characterization by Correlation of Various Photoelectron Spectroscopies: CO on W(110). *J. Electron Spectrosc. Relat. Phenom.* **1977**, *10*, 15–34. Umbach, E.; Menzel, D. An XPS study of Desorption and Dissociation Kinetics of CO on W(110). *Surf. Sci.* **1983**, *135*, 199–224.
- (42) Kim, Y. D.; Boo, J. H.; Lee, S. B. Adsorption Behaviors of CO on W(110) and Mo(110) Surfaces in the β-State Are Still Not Clear. *Surf. Sci.* **2009**, *603*, 1434–1438.
- (43) Bode, M.; Pascal, R.; Wiesendanger, R. STM Study of Carbon-Induced Reconstructions on W(110): Strong Evidence for a Surface Lattice Deformation. *Surf. Sci.* **1995**, *344*, 185–191.
- (44) Kohrt, C.; Gomer, R. Adsorption of CO on the (110) Plane of Tungsten: Temperature Dependence of the Sticking Coefficient and Absolute Surface Coverages. *Surf. Sci.* **1973**, *40*, 71–84.
- (45) Wang, C.; Gomer, R. Absolute Coverage Measurements: CO and Oxygen on the (110) Plane of Tungsten. *Surf. Sci.* **1978**, *74*, 389–404.
- (46) Steinbrückel, Ch.; Gomer, R. The Adsorption of CO on the (110) Plane of Tungsten: LEED, XPS and Auger Measurements. *Surf. Sci.* **1977**, *67*, 21–44.
- (47) Hwu, H. H.; Polizzetti, B. D.; Chen, J. G. Potential Application of Tungsten Carbides as Electrocatalysts: 2. Coadsorption of CO and H<sub>2</sub>O on Carbide-Modified W(111). *J. Phys. Chem. B* **2001**, *105*, 10045–10053.
- (48) Hwu, H. H.; Chen, J. G. Potential Application of Tungsten Carbides as Electrocatalysts: 4. Reactions of Methanol, Water and Carbon Monoxide over Carbide-Modified W(110). *J. Phys. Chem. B* **2003**, *107*, 2029–2039.
- (49) Benziger, J. B.; Ko, E. I.; Madix, R. J. The Characterization of Surface Carbides of Tungsten. *J. Catal.* **1978**, *54*, 414–425.
- (50) Brillo, J.; Sur, R.; Kuhlenbeck, H.; Freund, H. J. Interaction of CO and NO with WC(0001). *Surf. Sci.* **1998**, *397*, 137–144.

- (51) Brillo, J.; Hammoudeh, A.; Kuhlenbeck, H.; Panagiotides, N.; Schwegmann, S.; Over, H.; Freund, H. J. Structural Studies of WC(0001) and the Adsorption of Benzene. *Surf. Sci.* **1998**, *397*, 137–144.
- (52) Gottfried, J. M.; Schmidt, K. J.; Schroeder, S. L. M.; Christmann, K. Adsorption of Carbon Monoxide on Au(110)-(1 × 2). *Surf. Sci.* **2003**, *536*, 206–224.
- (53) Kim, J.; Samano, E.; Koel, B. E. CO Adsorption and Reaction on Clean and Oxygen-Covered Au(211) Surfaces. *J. Phys. Chem. B* **2006**, *110*, 17512–17517.
- (54) Ruggiero, C.; Hollins, P. Adsorption of Carbon Monoxide on the Gold (332) Surface. *J. Chem. Soc., Faraday Trans.* **1996**, *92*, 4829–4834.
- (55) Weststrate, C. J.; Lundgren, E.; Andersen, J. N.; Rienks, E. D. L.; Gluhoi, A. C.; Bakker, J. W.; Groot, I. M. N.; Nieuwenhuys, B. E. CO Adsorption on Au(310) and Au(321): 6-Fold Coordinated Gold Atoms. *Surf. Sci.* **2009**, *603*, 2152–2157.
- (56) Yim, W.; Nowitzki, T.; Necke, M.; Schnars, H.; Nickut, P.; Biener, J.; Biener, M. M.; Zielasek, V.; Al-Shamery, K.; Klüner, T.; Bäumer, M. Universal Phenomena of CO Adsorption on Gold Surfaces with Low-Coordinated Sites. *J. Phys. Chem. C* **2007**, *111*, 445–451.
- (57) Winkler, C.; Carew, A. J.; Haq, S.; Raval, R. Carbon Monoxide on  $\gamma$ -Alumina Single Crystal Surfaces with Gold Nanoparticles. *Langmuir* **2003**, *19*, 717–721.
- (58) Shaikhutdinov, S.; Meyer, R.; Naschitzki, M.; Bäumer, M.; Freund, H. J. Size and Support Effects for CO Adsorption on Gold Model Catalysts. *Catal. Lett.* **2003**, *86*, 211–219.
- (59) Outka, D. A.; Madix, R. J. The Oxidation of Carbon Monoxide on the Au(110) Surface. *Surf. Sci.* **1987**, *179*, 351–360.
- (60) Viswanath, Y.; Schmidt, L. D. Oxidation of Carbon on (100)W and (100)Mo. *J. Chem. Phys.* **1973**, *59*, 4184–4191.
- (61) Gottfried, J. M.; Schmidt, K. J.; Schroeder, S. L. M.; Christmann, K. Oxygen Chemisorption on Au(110)-(1 × 2). I. Thermal Desorption Measurements. *Surf. Sci.* **2003**, *525*, 184–196.
- (62) Stöhr, M.; Podloucky, R.; Müller, S. Ab-Initio Phase Diagram of Oxygen Adsorption on W(110). *J. Phys.: Condens. Matter* **2009**, *21*, 134017.
- (63) Deisl, C.; Swamy, K.; Bertel, E.; Meister, G.; Goldmann, A. Interaction of Ag and O on W(110) Studied by Scanning Tunneling Microscopy. *Surf. Sci.* **2006**, *600*, 2900–2906.
- (64) Zellner, M. B.; Chen, J. G. Surface Science and Electrochemical Studies of WC and W<sub>2</sub>C PVD Films as Potential Electrocatalysts. *Catal. Today* **2005**, *99*, 299–307.